Convergence and reliability of the Rehr-Albers formalism in multiple-scattering calculations of photoelectron diffraction

Y. Chen
Materials Sciences Division, Lawrence Berkeley National Laboratory, Berkeley, California 94720

F. J. García de Abajo
Department CCIA, Facultad de Informatica, Universidad del Pais Vasco/EHU, Apartado 649, 20080 San Sebastian, Spain

A. Chassé
Department of Physics, Martin-Luther-Universität, Halle-Wittenberg, D-06099 Halle (Saale), Germany

R. X. Ynzunza
Department of Physics, University of California at Davis, Davis, California 95616

A. P. Kaduwela*
Materials Sciences Division, Lawrence Berkeley National Laboratory, Berkeley, California 94720

M. A. Van Hove and C. S. Fadley
Materials Sciences Division, Lawrence Berkeley National Laboratory, Berkeley, California 94720
and Department of Physics, University of California at Davis, Davis, California 95616
(Received 19 June 1998)

The Rehr-Albers (RA) separable Green's-function formalism, which is based on an expansion series, has been successful in speeding up multiple-scattering cluster calculations for photoelectron diffraction simulations, particularly in its second-order version. The performance of this formalism is explored here in terms of computational speed, convergence over orders of multiple scattering, over orders of approximation, and over cluster size, by comparison with exact cluster-based formalisms. It is found that the second-order RA approximation [characterized by (6×6) scattering matrices] is adequate for many situations, particularly if the initial state from which photoemission occurs is of *s* or *p* type. For the most general and quantitative applications, higher-order versions of RA may become necessary for *d* initial states [third-order, i.e., (10×10) matrices] and *f* initial states [fourth-order, i.e., (15×15) matrices]. However, the required RA order decreases as an electron wave proceeds along a multiple-scattering path, and this can be exploited, together with the selective and automated cutoff of weakly contributing matrix elements and paths, to yield computer time savings of at least an order of magnitude with no significant loss of accuracy. Cluster sizes of up to approximately 100 atoms should be sufficient for most problems that require about 5% accuracy in diffracted intensities. Excellent sensitivity to structure is seen in comparisons of second-order theory with variable geometry to exact theory as a fictitious ''experiment.'' Our implementation of the Rehr-Albers formalism thus represents a versatile, quantitative, and efficient method for the accurate simulation of photoelectron diffraction.
[S0163-1829(98)04943-1]

I. INTRODUCTION

The technique of core-level photoelectron diffraction (PD) has been applied to surface structure determination on the atomic scale for more than 20 years.[1] This local diffraction technique probes short-range order around the emitter. A broad variety of surfaces have been successfully studied, including metals, semiconductors, oxides, systems exhibiting surface core-level shifts, adsorbed atoms and molecules, epitaxial overlayers, and atoms at buried interfaces. A number of research groups have performed photoelectron diffraction experiments to study surface and interface structures, using both laboratory x-ray and synchrotron radiation sources, and doing the measurements in both scanned-angle and scanned-energy modes. Several reviews of this field have appeared in recent years.[2–8] A further element that has recently been added to this technique is the application of holographic inversion methods to photoelectron diffraction data so as to more directly yield atomic structures in three dimensions.[9–18] Thus, the accurate theoretical modeling of photoelectron diffraction is crucial to the development and use of this technique in its various forms, and we here critically discuss one particularly attractive method for accomplishing this.

In core-level photoemission, a photon illuminates an emitting atom at or near the surface or in the solid and excites an electron from an atomic core level, ejecting the electron to a detector far away from the surface (the far-field limit). The resulting photoelectron wave components can occur both by direct propagation to the far-field detector and via a number of scatterings from atoms in the neighborhood of the emitter. The quantum interference (diffraction) between the different pathways depends sensitively on the relative atomic posi-

tions. The intensity associated with this process, when measured as a function of photon energy and/or emission angles, thus includes information about the atomic structure around the emitter. The energy- and angle-resolved photoemission intensity $I(\mathbf{k},\theta,\phi)$ at the detector can be written in general as

$$I(\mathbf{k},\theta,\phi) \propto \left| \phi_0 + \sum_j \phi_{s_j} \right|^2, \tag{1}$$

where $\mathbf{k}$ is the final electron wave vector (related to the final kinetic energy), θ and ϕ are the polar and azimuthal angles of photoelectron emission, respectively, ϕ_0 is the wave component representing travel along a path directly to the detector without being scattered by another atom, and ϕ_{sj} is the wave component representing travel via paths involving single or multiple scattering by one or more atoms, respectively. The multiple-scattering order is defined as the number of scattering atoms in a path: $j=1$ is single, 2 is double, etc. Higher-order scattering processes are less important because of the roughly $1/r$ falloff of the outgoing distorted spherical wave represented by ϕ_0, damping due to inelastic processes and loss of diffraction modulation due to thermal vibrations (Debye-Waller effects). The explicit sum in Eq. (1) includes all possible scattering paths inside the solid.

To briefly review the history of such theoretical modeling of PD effects, the first qualitative analyses of higher-energy data made use of Kikuchi-band theory.[19–23] An early quantitative theoretical explanation of these diffraction data was provided by Liebsch in 1974 (Ref. 24) and then improved on by him and others with multiple-scattering effects in 1976;[25,26] it was based on LEED theory. In the next few years, Pendry,[27] as well as Li, Lubinsky, and Tong,[28] put forward similar theories involving the more complex nature of both the initial and final states. These theories require the assumption of full translational symmetry parallel to the surface for the system under investigation.

A single-scattering cluster-based theory based on prior work in extended x-ray absorption fine structure (EXAFS) and preliminary work on Auger electron diffraction (AED) was first applied to scanned-angle photoelectron diffraction by Kono *et al.*;[29–31] this was based on the plane-wave approximation., The next major advance in the cluster approach was by Barton and Shirley,[32,33] who included both spherical-wave corrections and multiple scattering effects. The cluster-based theories are inherently more suitable for photoelectron diffraction modeling in view of the point-source nature of the problem, the spherical outgoing waves involved, the short inelastic attenuation lengths, and the sensitivity to short-range rather than long-range order. In particular, one key advantage of PD as a structure probe is in not requiring long-range translational order, and so being able to model such short-range order structures conveniently without having to resort to some sort of repeated structure with fictitious long-range order is crucial. Cluster-based methods are ideal for this. It has also been found that the maximum cluster size required for accurate simulations is about 100 atoms.[2–4]

The multiple scattering expansion for spherically symmetric scatterers is conveniently formulated in terms of diagonal plane-wave scattering t matrices with elements t_l

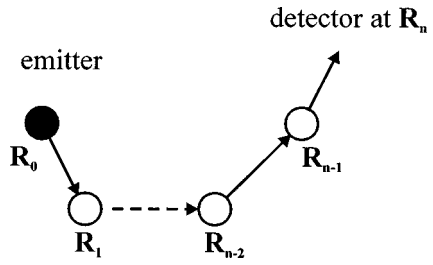

FIG. 1. A photoelectron excited from the core level of an emitter atom at $\mathbf{R}_0$ propagates to the detector at $\mathbf{R}_n$ via $n-1$ scatterers $\mathbf{R}_1,\mathbf{R}_2,\ldots,$ and $\mathbf{R}_{n-1}$. Each straight segment linking consecutive atoms represents a Green's-function propagator $G_{LL}[k(\mathbf{R}_{i+1}-\mathbf{R}_i)]$. The emitter can become a scatterer after emission.

$=\sin(\delta_l)\exp(i\delta_l)$ and matrix elements of the free-particle propagator $G_{L,L'}(\rho)=\langle L,\mathbf{R}|G|L',\mathbf{R}'\rangle$ in an angular momentum $L=(l,m)$ and site basis $|L,\mathbf{R}\rangle$. Here $\rho=k(\mathbf{R}-\mathbf{R}')$ denotes the dimensionless vector between two sites, $k=|\mathbf{k}|$ is the wave number. $G_{LL'}(\rho)$ is defined by the following integral[34] involving spherical Bessel functions $j_1(kr)$ and spherical harmonics $Y_L(\hat{\mathbf{k}})$:

$$G_{LL'}(\rho) = -\frac{(4\pi)^2}{2k} \times \int \frac{d^3\mathbf{k}}{(2\pi)^3} \frac{Y_L^*(\hat{\mathbf{k}})Y_{L'}(\hat{\mathbf{k}})\exp(i\mathbf{k}\cdot(\mathbf{R}-\mathbf{R}')}{\varepsilon - k^2/2 + i0^+} \times \frac{j_l(kr)j_{l'}(kr')}{j_l(\sqrt{2\varepsilon}r)j_{l'}(\sqrt{2\varepsilon}r')}, \tag{2}$$

where $\hat{\mathbf{k}}$ is a unit vector along $\mathbf{k}$, r and r' are arbitrary displacements. An $(n-1)$-atom path (Fig. 1), including the emitter atom at R_0, $n-1$ scatterers at $\mathbf{R}_1,\mathbf{R}_2,\ldots,\mathbf{R}_{n-1}$, and the detector at $\mathbf{R}_n$ is represented by the following total propagator in this *exact multiple-scattering expansion*:

$$\begin{aligned} G^{(n-1)}_{L_n,L_0}(\mathbf{R}_0,\mathbf{R}_1,\mathbf{R}_2,\ldots,\mathbf{R}_n) = \sum_{(\text{paths})} \sum_{\{L_i\}} & G_{L_n,L_{n-1}}(\rho_n) \\ & \times t_{ln-1}(\mathbf{R}_{n-1}) \\ & \times G_{L_{n-1},L_{n-2}}(\rho_{n-1})\cdots \\ & \times t_{l_2}(\mathbf{R}_2) \\ & \times G_{L_2,L_1}(\rho_2)t_{l_1}(\mathbf{R}_1) \\ & \times G_{L_1,L_0}(\rho_1), \end{aligned} \tag{3}$$

where $\rho_i=k(\mathbf{R}_{i+1}-\mathbf{R}_i)$, and L_0 and L_n denote fixed initial and final angular momenta.

Several computer programs have been written to successfully calculate photoelectron diffraction intensities based on this exact cluster formalism, for example, by Chassé and co-workers[35,36] and by García de Abajo.[37] However, without special optimization (as we consider below) such exact programs in general require considerable computing times for large clusters, due to the large matrix dimensions involved and the large number of paths that are explicitly summed over. That is, the matrix $G_{LL'}$ has dimensions $(l_{\max}+1)^2$

$\times(l_{\max}+1)^2$, where $l_{\max}$ is the largest angular momentum value needed to accurately represent scattering, and can be roughly evaluated using $l_{\max}\sim k_{\max}R_{\mathrm{mt}}$, where R_{mt} is the muffin-tin radius of the scattering potential. For photoelectron diffraction in the energy range 50–1500 eV, this $l_{\max}$ lies between 5 and 30, respectively, of course depending on the electron energy. The computing time can be considerably reduced by an iterative summing over the multiple-scattering paths, as proposed by García de Abajo,[37] which leads to proportionality to the number of multiple scatterings, rather than the much steeper behavior as in the traditional summing method. More precisely, the total calculation time in traditional summing is $T\propto T_2^{n_{\max}/2}$, while the iterative summing has a total time of $T\propto n_{\max}T_2$, where T_2 is the time for a double scattering calculation, and $n_{\max}$ is the maximum multiple-scattering order included. A convergent calculation is found to require $n_{\max}$ up to about 6, or even higher in cases with long straight chains for strongly forward scattering atoms. We have used these two ''exact'' formalisms in the present work as references with which to compare our Rehr-Albers calculations.

Several methods have been proposed previously for approximating the exact scattering formalism so as to reduce computation times in cluster calculations.

(i) Barton and Shirley first derived a representation of the exact formalism with their Taylor-series magnetic-quantum-number expansion (MQNE).[38] This reduces the matrix dimension that needs to be used, since only the first three Taylor orders are usually required.

(ii) Fritzsche, Rennert, and Chassé[39–41] provided a reduced angular momentum expansion (RAME) approximation. The incoming spherical waves are approximated by a limited set of spherical harmonics with low angular momenta [quantum numbers $(l,m)=(0,0)$, $(1,-1)$, $(1,0)$ and $(1,1)$]. Improvement has been achieved[41] by taking into account two more components of higher angular momenta $(l,m)=(2,0)$ and $(3,0)$. A generalized scattering amplitude of each scattering process contains curved wave corrections and a rotation operator that rotates the z axis between the wave vectors before and after the scattering.

(iii) As another approach to reduce computation times, Rehr and Albers developed a theory, denoted RA in this paper, that is based on a separable representation of the exact formalism; it was developed primarily to calculate NEXAFS (near-edge x-ray-absorption fine structure) and EXAFS (extended x-ray absorption fine structure).[42] Curved-wave multiple-scattering contributions can in this approach be calculated with an efficient formalism similar to that based on the plane-wave approximation, but with scattering amplitudes replaced by distance-dependent scattering matrices that act like effective scattering factors. A useful property of this method is that the size of the scattering matrices can be systematically increased as needed for sufficient accuracy, ultimately recovering the exact result. Thereby, the successive orders of scattering can be built up and convergence be achieved in a convenient and efficient way. The first application of this theory to photoelectron diffraction was in a computer program developed by Kaduwela, Friedman, and Fadley,[43] and this was based on the second order of the RA approximation, i.e., scattering matrices of dimension (6×6).

(iv) In a more recent development based on the RA approach, Wu, Chen, and Shirley[44] developed a faster program that benefits from a novel reverse-summation method over paths and an iterative summing technique, but is again limited to second order in RA. Chen and Van Hove have further developed this method to enable the inclusion up to fourth order in RA [up to (15×15) matrices]. By an efficient path-cut process, this program runs even faster. The resulting computer package, called MSCD is also very portable, running on a variety of sequential and parallel computers.[45]

In this paper, we briefly introduce both the exact and RA formalisms, discuss the methods that have been used to increase the calculational efficiency of RA, present a number of results calculated with the MSCD program based on RA and compare these results with exact cluster calculations to quantitatively evaluate the performance and limitations of the RA approximation as carried out to different orders. Section II discusses a few more necessary details about the exact cluster-based formalism. Section III briefly reviews the RA method and its properties. The methodology and convergence of the implementation of RA used in the MSCD program is explored in Sec. IV. The overall reliability of the MSCD approach for structural determinations is covered in Sec. V, and our conclusions are presented in Sec. VI.

II. EXACT REPRESENTATION OF THE PROPAGATOR

The term ''exact'' in this paper means that no RA approximation is made, or rather that, even if a RA expansion is used, it is carried to all orders, since it will in principle converge to the ''exact'' result. We note in this context that Brouder and Sébilleau have shown that the RA representation carried to all orders turns out to be an accurate, stable, and efficient way to calculate the exact propagator.[46,47]

For simplicity in the formulas presented in this paper, we do not include effects due to inelastic scattering or vibrational motion, even though it is clear that these effects are essential for a quantitative description of experimental data. Both of these effects tend to damp out scattering from atoms further from the emitter, thus causing multiple-scattering paths to be effectively reduced in length. Both of these effects are, however, included in our MSCD programs and in some of the calculations presented in this paper. Using the exact propagator, Eq. (3), and the same notation conventions as in Ref. 43, the multiple scattering photoemission intensity can be expressed as [Eq. (41) of Ref. 43]

$$I_{n_il_i}^{(n_{\max})}(k,\theta,\phi)\propto\sum_{\text{emitter}}\sum_{m_i}\left|\sum_{l_f=l_i\pm1}m_{l_f,c}\exp(i\,\delta_{l_f,c})\times\left[G_{00,l_fm_i}^{(0)}(\mathbf{R}_0,\mathbf{R}_d)+G_{00,l_fm_i}^{(1)}(\mathbf{R}_0,\mathbf{R}_1,\mathbf{R}_d)+\sum_{n=3}^{n_{\max}}G_{00,l_fm_i}^{(n-1)}(\mathbf{R}_0,\mathbf{R}_1,\mathbf{R}_2,\ldots,\mathbf{R}_{n-1},\mathbf{R}_d)\right]\right|^2, \tag{4}$$

where $I_{n_il_i}^{(n_{\max})}(k,\theta,\phi)$ is the photoemission intensity from electronic subshell (n_i,l_i), as detected with wave vector k in the (θ,ϕ) direction; (n_i,l_i,m_i) are the quantum numbers of the

initial core orbital ($n_i=1,2,3,4,\ldots=K,L,M,N,\ldots$ shells, respectively, $l_i=0,1,2,3,...=s,p,d,f,\ldots$ subshells, and m_i is the magnetic quantum number); and $L_f=(l_f,m_f)$ are angular momentum quantum numbers of the final state. The dipole selection rules imply $l_f-l_i=\pm 1$, $m_f-m_i=0$, where we for simplicity restrict ourselves to linear polarized incident light, although this can be generalized in a straightforward way to other polarizations, such as circular or elliptical.[48] $G^{(n-l)}_{00,l_f m_i}(\mathbf{R}_0,\mathbf{R}_1,\mathbf{R}_2,\ldots,\mathbf{R}_{n-1},\mathbf{R}_d)$ is the exact nth-order multiple scattering Green's function for a scattering path from the emitter at $\mathbf{R}_0\equiv\mathbf{R}_{\text{emitter}}$ via scatterers at $\mathbf{R}_1,\mathbf{R}_2\ldots,\mathbf{R}_{n-1}$ to the detector at $\mathbf{R}_n\equiv\mathbf{R}_{\text{detector}}\equiv\mathbf{R}_d$. The quantities $m_{l_f,c}$ and $\delta_{l_f,c}$ are the amplitude and phase of the dipole matrix element into a given final state, and are related to the short-range central potential of the ionized atom; that is, the long-range Coulomb field is neglected due to the assumed screening of the core hole near a solid surface.[49] The quantities $m_{l_f,c}$ and $\delta_{l_f,c}$ are calculated from $\langle\Psi_{E_{\text{kin}},l_f}|\boldsymbol{\varepsilon}\cdot\mathbf{r}|\phi_{n_i l_i}\rangle$, with $\Psi_{E_{\text{kin}},l_f}$ being the final continuum state of the photoelectron at a kinetic energy E_{kin} and propagating in direction $\mathbf{r}$, $\phi_{n_i l_i}$ is the initial core orbital $L_i=(l_i,m_i)$ from which the photoelectron is emitted, and $\boldsymbol{\varepsilon}$ is the radiation polarization vector. The summations run over all emitters, all final states $L_f=(l_f,m_f)$ and over all combinations of order n, the number of scatterers (number of atoms$=n+1$) in a given scattering path from single scattering ($n=1$) to the highest order considered $n=n_{\max}$ (typically we select $n_{\max}=8$ or higher, corresponding to 7 or more scattering events).

Now we choose the $\mathbf{z}$ direction to be parallel to the $\boldsymbol{\varepsilon}$ vector to simplify the matrix element evaluation. The expression for the matrix element then becomes [Eq. (6) of Ref. 43],

$$m_{l_f,c}=(-i)^{l_f}\langle R_{E_{\text{kin}},l_f}(r)|r|R_{n_i,l_i}(r)\rangle \times\langle Y_{l_f,m_i}(\theta,\phi)|Y_{10}(\theta,\phi)|Y_{l_i,m_i}(\theta,\phi)\rangle, \quad (5)$$

where $R_{E_{\text{kin}},l_f}(r)$ is the radial part of the continuum orbital at l_f, $R_{n_i l_i}(r)$ is the radial part of the initial core orbital with quantum numbers n_i and l_i, and $Y_{lm}(\theta,\phi)$ are the relevant spherical harmonics.

III. SEPARABLE REPRESENTATION OF THE PROPAGATOR

In the convergent separable representation of the propagator derived by Rehr and Albers, the exact propagator $G_{LL'}$ is rewritten as[42]

$$G_{LL'}(\rho)=\frac{\exp(i|\rho|)}{|\rho|}\sum_{\lambda}\tilde{\Gamma}^{L}_{\lambda}(\rho)\Gamma^{L'}_{\lambda}(\rho), \quad (6)$$

where a new combination index $\lambda=(\mu,\nu)$ is introduced, such that, for an exact representation, $\mu=-l_{\max}$ to $l_{\max}$, and $\nu=0$ to $|\mu|$. However, this expansion converges relatively quickly, and can usually be truncated without significant loss of accuracy, as we shall show in Sec. IV B. The $\Gamma^{L}_{\lambda}(\rho)$ and $\tilde{\Gamma}^{L}_{\lambda}(\rho)$ have the following forms:

$$\Gamma^{L}_{\lambda}(\rho)=(-1)^{\mu}N_{l\mu}\frac{C_l^{(|\mu|+\nu)}(z)}{(|\mu|+\nu)!}z^{|\mu|+\nu}R^{l}_{\mu m}(\Omega_p), \quad (7)$$

$$\tilde{\Gamma}^{L}_{\lambda}(\rho)=R^{l}_{m\mu}(\Omega_\rho^{-1})\frac{(2l+1)}{N_{l\mu}}\frac{C_l^{(\nu)}(z)}{\nu!}z^{\nu} \quad (8)$$

with

$$N_{l\mu}=[(2l+1)(l-|\mu|)!/(l+|\mu|)!]^{1/2}, \quad (9)$$

$$C_l^{\nu}(z)=\frac{d^{\nu}}{dz^{\nu}}C_l(z). \quad (10)$$

Here $z=1/(i|\rho|)$, $C_l(z)$ is the degree-l polynomial factor of the spherical Hankel function, $R^{l}_{\mu m}(\Omega_\rho)$ is a matrix that rotates the bond direction ρ onto the $\mathbf{z}$ axis, Ω_ρ represents the Euler angles for this rotation. The $R^{l}_{\mu m}(\Omega_\rho)$ transforms the spherical harmonics as

$$Y_{lm}(\hat{\mathbf{k}})=\sum_{m'}Y_{lm'}(\hat{\mathbf{k}}')R^{l}_{m'm}(\Omega_p). \quad (11)$$

Substituting Eq. (6) into Eq. (3), one thus obtains the exact equivalent form

$$G^{(n-1)}_{00,L_f}(\mathbf{R}_1,\mathbf{R}_2,\ldots,\mathbf{R}_n)=\sum_{(\text{paths})}\sum_{\{\lambda_i\}}\tilde{\Gamma}^{00}_{\lambda_n}(\rho_n)\times F_{\lambda_n,\lambda_{n-1}}(\rho_n,\rho_{n-1})\cdots\times F_{\lambda_3,\lambda_2}(\rho_3,\rho_2)F_{\lambda_2,\lambda_1}(\rho_2,\rho_1)\times\Gamma^{L_f}_{\lambda_l}(\rho_1). \quad (12)$$

This is the Rehr-Albers separable representation formula for curved-wave multiple-scattering, which is a direct analog of the plane-wave approximation[50] or the point-scattering approximation.[51]

In Eq. (12), the *scattering-amplitude matrices* $F_{\lambda_j,\lambda_{j-1}}(\rho_j,\rho_{j-1})$ at each site are defined in the partial-wave expansion as

$$F_{\lambda\lambda'}(\rho,\rho')=\frac{\exp(i|\rho'|)}{|\rho'|}\sum_{L}t_l\Gamma^{L}_{\lambda}(\rho)\tilde{\Gamma}^{L'}_{gl'}(\rho'), \quad (13)$$

where ρ' and ρ are the interatomic vectors leading from and to the site, as illustrated in Fig. 2. The sum on L runs over both l and m quantum numbers.

The RA representation, Eq. (13), is thus an exact formula if we take all the possible $\lambda=(\mu\nu)$ values into account. But in practice, noting the asymptotic form $F_{\lambda\lambda'}\propto(\rho)^{-(2\nu+\mu)}(\rho')^{-(2\nu'+\mu')}$ for large ρ' and ρ, we can safely truncate $F_{\lambda\lambda'}$ at different approximation orders. Table I lists, as a function of the RA approximation order, the dimensions of the scattering-amplitude matrices, and their possible (μ,ν) values. For most real cases that we have encountered, it was found that second order [(6×6) matrices] is adequate to simulate experimental curves,[43] and this will be further investigated in this paper.

The advantage of the RA representation is that the approximation leads to smaller matrix sizes, resulting in much reduced computation times. In the exact formalism, Eq. (3),

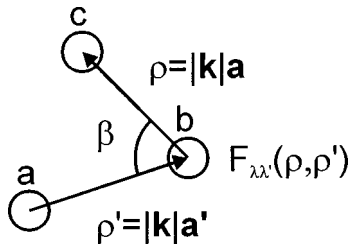

FIG. 2. A scattering event leading from atom a to atom c via atom b. The $\rho' = k\mathbf{a}'$ and $\rho = k\mathbf{a}$ are the dimensionless interatomic vectors leading from and to the site in question, with $\mathbf{a}'$ and $\mathbf{a}$ the corresponding vectors and k the wave number ($k=|\mathbf{k}|$, $\mathbf{k}$ is the wave vector), while β is the angle between the interatomic vectors ρ' and ρ. The quantity $F_{\lambda\lambda'}(\rho,\rho')$ is the effective scattering amplitude via the Rehr-Albers approximation.

the propagator matrix $G_{LL'}$ has the dimensions $(l_{\max}+1)^2 \times (l_{\max}+1)^2$, where $l_{\max}$ can be estimated as described previously and for a typical muffin-tin radius R_{mt} of 1.5 Å yields matrix sizes of (36×36) and (441×441). By contrast, in most cases, the RA representation requires matrix sizes of only (6×6), although we discuss below some cases where going up to (15×15) might be required for ultimate quantitative accuracy.

IV. CONVERGENCE

There are several nonstructural parameters that need to be taken to convergence when using the RA representation in photoelectron diffraction simulations: the cluster size n_{cluster}, the multiple-scattering order $n_{\max}$, the RA order $|\mu|_{\max}$, and the maximum angular momentum $l_{\max}$. In order to carry out such converged calculations most efficiently, we also include or exclude paths based on their relative importance through a control parameter *pathcut*, as explained in more detail below. All of these parameters except the RA order also occur in the exact cluster methods. In this section, we address the importance of each of these parameters through a series of calculations. By default, the following quantities were chosen for all the calculations, with variations as specified in subsequent subsections.

The calculations are performed for a default cluster of 86 atoms representing the ideal clean Cu(111) surface, using a lattice constant of 3.615 Å. Intensities are thus summed over emitters in various layers inward from the surface. The cluster shape is chosen to be a half-ellipsoid, as shown in Fig. 3, with $r=7$ Å and $h=8$ Å and the emitter in each layer is positioned as close as possible to the lateral center of it.

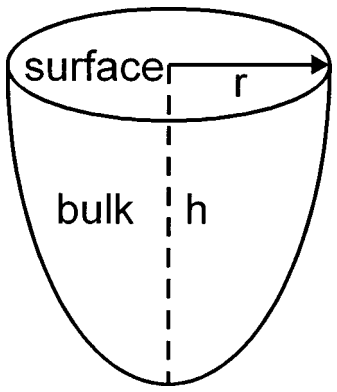

FIG. 3. Cluster shape selection using a half ellipsoid. The side view is a semiellipse with minor axis r and major axis h. The top view is a circle with radius r. For the 86-atom cluster used to simulate Cu(111), h was 8 Å or 4 emitter layers in depth, and r was 7 Å.

Scattering phase shifts and radial matrix elements are calculated from a muffin-tin potential due to Moruzzi *et al.*,[52] which uses a 1.26-Å muffin-tin radius; this leads to $l_{\max}\approx 7$ and 13 for electron kinetic energies of 100 and 400 eV, respectively. The inelastic attenuation length is calculated using the TPP-2M formula of Tanuma, Powell, and Penn,[53,54] which yields about 4.4 Å at an energy of 100 eV and 8.5 Å at 400 eV. No thermal vibrational damping effect is included. The inner potential was assumed to be 0 eV for these model calculations, thus neglecting any photoelectron refraction effects in crossing the surface barrier. Of course, in any actual comparison with experiment, this parameter should be set to some reasonable nonzero value. A linearly polarized light source illuminates the surface along a [110] azimuth and at a grazing incidence angle of 10 ° (i.e., 80° from normal) so that the polarization lies nearly along the surface normal. Photoemission signals are taken from the Cu $3p$ initial state. By default, we set $n_{\max}=8$, the RA order$=4$ $(15\times 15$ matrices), $l_{\max}=20$, and the *pathcut* (to be defined more quantitatively below)$=0.01$. Unless otherwise noted these are the values used in all calculations to systematically study parameter choices.

A. Multiple-scattering order $n_{\max}$

In general, photoelectrons are scattered less to large scattering angles than near forward scattering (scattering angle of 0), as illustrated for energies of 156 and 547 eV for a single Cu scatterer in Fig. 4. This implies that multiple forward scattering along dense rows of atoms in a crystal can be

TABLE I. Rehr-Albers approximation orders, dimensions of the corresponding scattering-amplitude matrices, and allowed values of (μ,ν).

RA order	F matrix dimension	(μ,ν)
0	1×1	(0,0)
1	3×3	(0,0), (±1,0)
2	6×6	(0,0), (±1,0), (0,1), (±2,0)
3	10×10	(0,0), (±1,0), (0,1), (±2,0), (±1,1), (±3,0)
4	15×15	(0,0), (±1,0), (0,1), (±2,0), (±1,1), (±3,0), (0,2), (±2,1), (±4,0)

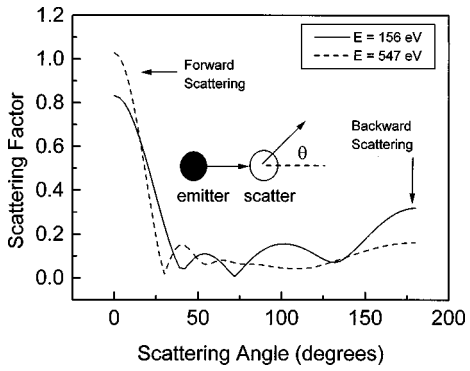

FIG. 4. Cu elastic scattering factors vs scattering angle θ at photoelectron kinetic energies 156 and 547 eV (wave numbers 6.4 and 12.0 Å^{-1}). These scattering factors are calculated via the spherical-wave 2-atom cluster with 2.5-Å distance.

particularly strong, e.g., for deeper emitters farther from the surface of the cluster. In order to explore the influence of scattering order, the photoelectron detector is thus placed to receive electrons emitted 35.23 ° off the [111] normal and along a [110] nearest-neighbor forward-scattering direction in the fcc lattice. No angular broadening due to the effective detector aperture was included and kinetic energies of 156 and 547 eV (wave numbers $k=6.4$ and 12.0 Å^{-1}) were studied.

Figure 5 shows the convergence of photoelectron diffraction intensities as a function of multiple-scattering orders, for two typical energies, calculated with $(|\mu|+2\nu)_{\max}=4$, i.e., in fourth order of RA, (15×15) matrix, as compared with exact (i.e., non-RA) calculations for the same conditions. In these calculations, the emitter is put on the third layer, so that the maximum number of forward scatterers along the direction chosen is two. A photoelectron can thus be scattered once or twice consecutively along with the forward-scattering path from emitter to detector. After the sixth order of multiple scattering, the intensities have essentially converged within a few percent, and the fourth-order RA is essentially identical to the exact results. The same sort of convergence can also be seen in Fig. 6 when the emitter is

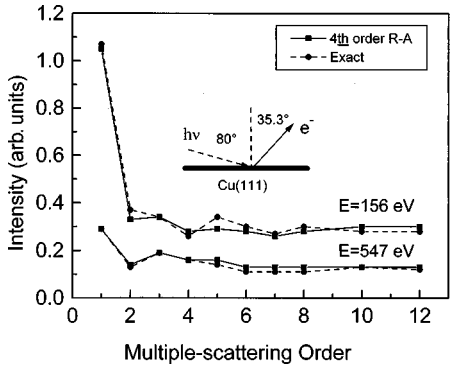

FIG. 5. Calculated Cu 3*p* photoelectron intensities, as a function of multiple scattering order, from clean Cu(111) in a fixed forward-scattering emission direction, 35.23° off-normal, and for emission from the third layer. A photoelectron can be scattered once or twice consecutively along this forward-scattering path. Photoelectron energies are 156 and 547 eV. Default values are used for other parameters. The fourth order RA is compared with exact calculations.

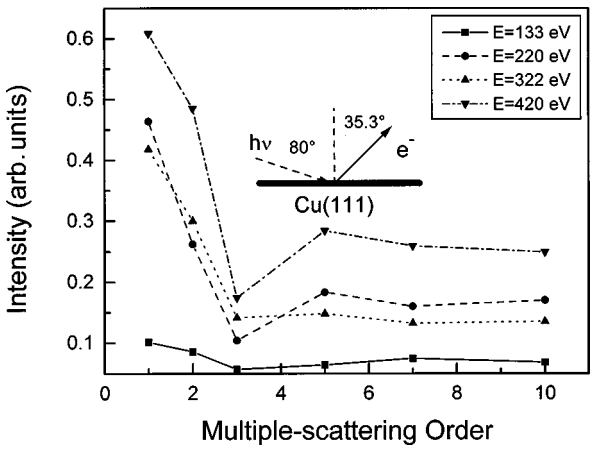

FIG. 6. Same as Fig. 5, but for emission from the fourth layer. A photoelectron can be scattered up to three times consecutively along this forward-scattering path. Four different photoelectron energies are considered. No exact results were calculated.

moved into the fourth layer and the forward-scattering path has three scattering atoms; here, seventh order appears necessary to ensure convergence. No exact results are shown here due to prohibitive computational times with the nonoptimized program utilized. Earlier test calculations by Kaduwela *et al.* with the RA methods investigated multiple scattering along long straight chains of atoms and showed similar results.[43] The addition of thermal vibration effects should also reduce off-forward scattering amplitudes, thereby aiding the convergence of the multiple scattering series. Finally, any experimental angular averaging will tend to smear out sharper diffraction features associated with longer path length differences, further acting to enhance convergence.

We thus conclude that fourth order RA is essentially equal to exact, and that the maximum order of scattering needed to adequately simulate PD patterns is sixth or seventh, but probably lower than this with the inclusion of vibrational effects and angular averaging. This agrees with prior studies that have generally concluded that going to fourth or fifth order is sufficient.[33,34,43]

B. Rehr-Albers approximation order $|\mu|_{\max}$ and initial-state effects

To perform a stringent test of the RA order, we choose a cluster of 2 Cu atoms with an arbitrary small 2.0-Å bond length (somewhat less than the actual 2.56-Å nearest-neighbor distance in Cu), because it provides the maximum sensitivity to different approximation orders. Calculations using a more realistic bond length would converge more rapidly. Closely connected to the required RA order is the dependence of the RA approximation on the initial-state angular momentum: the 2-atom cluster also provides a good test of this question. A variety of calculations showed that low energies and single scattering are sufficient for this investigation.

Figure 7 shows scanned-angle photoelectron diffraction intensities for low-energy electrons ($E=61$ eV) as a function of scattering angle away from the interatomic axis in the 2-atom cluster. The polarization of the light is here taken to

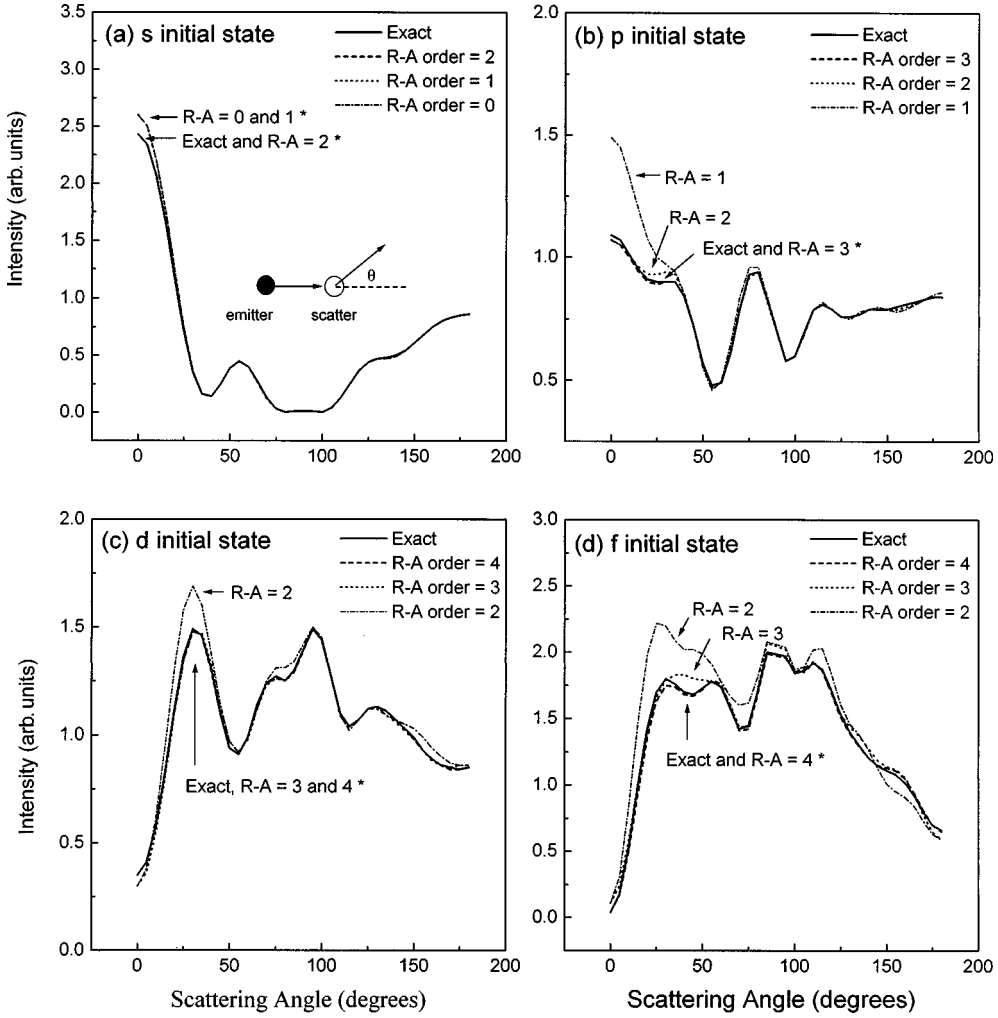

FIG. 7. Single scattering intensities from a 2 Cu-atom cluster with 2.0-Å interatomic spacing and for scattering angles varying between forward (0 °) and backward scattering (180 °). Emission from four different initial states, *s*, *p*, *d*, and *f*, is considered in panels (a), (b), (c), and (d), respectively. Default values are used for other parameters. Curves labeled with ∗ in each panel are visually identical.

be along the interatomic axis, in order to correspond to those atoms that are in general illuminated most strongly by the primary outgoing wave. Here $\theta=0°$ means forward scattering, while $\theta=180°$ corresponds to backward scattering. The four panels in Fig. 7 correspond to excitation from different initial states: $s(l_i=0)$, $p(l_i=1)$, $d(l_i=2)$, and $f(l_i=3)$; and in each panel we compare different RA orders with exact results under the same conditions. It is seen that for an *s* initial state emitting into *p* photoelectron waves, the first RA order $[(3\times3)$ matrices] is adequate and essentially identical to exact. For a *p* initial state emitting into *s* and *d* waves, the second RA order (6×6) is sufficient. For a *d* initial state emitting into *p* and *f* waves, the third RA order (10×10) might be needed. And for an *f* initial state emitting into *d* and *g* waves, the fourth RA order (15×15) is necessary to obtain results accurate within 1%. Here, it was found that changing the initial angular momentum had a strong effect on the diffraction patterns for a two-atom cluster, but the effect of RA order was not considered. As we shall discuss later, in a larger cluster, subsequent scatterings can be treated with equal or, more frequently lower, order in RA, so that the RA order needed for the first scattering is an upper limit for the entire multiple-scattering problem, and does not indicate the real limit on computing time for a given problem.

Overall, we thus suggest a simple rule of thumb for guaranteeing adequate results: for emission from an initial state l_i use the (l_i+1)th RA order for the first scattering event after emission. Other subsequent events will generally require lower orders, as dealt with in more detail in the next section.

C. Pathcut

Our MSCD RA codes include the ability to neglect multiple-scattering paths that contribute only weakly to the final photoemitted intensities. At the same time, they also allow the RA order to be adjusted at each stage in a scattering path, a unique feature not utilized before in PD simulations. Both options are controlled by one criterion, called *pathcut*, which is a cutoff criterion with value $\ll1$. In this section, we indicate how this cutoff has been implemented and explore the resulting compromises between time savings and accuracy.

The *pathcut* criterion is applied as follows. Before starting a multiple-scattering calculation, all individual single-center scattering events involving a three-atom ''vertex'' $a\rightarrow b\rightarrow c$ and represented by a given $F_{\lambda\lambda}(\rho,\rho')$ of the type shown in Fig. 2 are evaluated separately. The largest value of $F_{00}(\rho,\rho')$ is taken as the reference value. All those elements

TABLE II. Distribution (in percent) of different scattering amplitude matrix sizes as a function of multiple-scattering order (MS order) for an 86-atom Cu cluster with path cut of 0.001, using default values at energy $E=100$ eV. The column labeled ''none'' represents weak events that terminate a path.

MS order	RA order (matrix size)					
	none	0 (1×1)	1 (3×3)	2 (6×6)	3 (10×10)	4 (15×15)
1	0.0	0.0	0.0	0.0	0.0	100.0
2	0.0	1.1	39.3	43.2	7.6	8.7
3	33.6	53.5	12.1	0.7	0.1	0.0
4	27.3	32.3	5.3	0.5	0.0	0.0
5	61.9	20.1	3.0	0.3	0.0	0.0
6	83.8	13.7	2.2	0.3	0.0	0.0
7	87.6	10.3	1.8	0.3	0.0	0.0
8	89.7	8.3	1.7	0.3	0.0	0.0

$F_{\lambda\lambda'}(\rho,\rho')$ that are smaller than a factor *pathcut* times this largest $F_{00}(\rho,\rho')$ are declared to be negligible; this is done dynamically in a multiple-scattering path, so that scattering events further down a path, which are normally weaker because of decay with distance, will be cut off relatively more than early scattering events. In this way, a scattering matrix is automatically reduced as appropriate to a lower-order RA event with smaller matrix size and faster computation. In particular, if all elements of a matrix are declared negligible, the path is terminated. Because single scattering usually dominates, single scattering paths are calculated using *pathcut*=0.

To illustrate the effects of *pathcut* for a typical large-cluster case, we show in Table II a summary of results for multilayer emission from an 86-atom Cu(111) cluster at an energy of 100 eV, including the statistical weights in percent of scattering-amplitude matrix sizes when *pathcut*=0.001 (a typical value that we have found to represent a good compromise between computation time and accuracy). Although second-order multiple scattering requires dealing in about 16% of the cases with third and fourth order RA or matrices of (10×10) and (15×15) size, for third and higher multiple scattering order, second order RA and (6×6) matrices are found to be fully adequate. In fact, for fifth or higher multiple scattering order, first order RA is probably adequate. To further quantify the effect of *pathcut* on the quality of the resulting photoemitted intensities, we define an intensity reliability factor R_I as

$$R_I=\sum_i \frac{[I_i(pathcut=0)-I_i(pathcut)]^2}{I_i^2(pathcut=0)+I_i^2(pathcut)}, \qquad (14)$$

where I_i represents photoemission intensities, and the sum runs over all the available data points for different energies or angles. Thus $R_I=0$ represents a perfect calculation, as defined by *pathcut*=0.

Figure 8 shows the intensity reliability and calculation time as a function of *pathcut* for an energy scan of Cu 3*p* intensity over the energy range 60–550 eV for our 86-atom Cu(111) cluster. It can be seen that setting a *pathcut* value of 0.001 can easily save an order of magnitude of computation time compared to the full calculation without cut (*pathcut* =0), and also that a great deal of time gain is achieved even with this small a cutoff criterion. That is, going from 0 to 0.001 gains by a factor of about 19, whereas going from 0 to 0.01 gains by about 75. Figure 9 gives us a feeling for the quality of curve-to-curve comparisons at different *pathcut* values.

From this analysis and other calculations, we find that a *pathcut* value of 0.001 is fully adequate for the quantitative modeling of photoelectron diffraction data.

D. Cluster size

If a cluster is to represent an infinitely extended surface and/or include multilayer emission from a bulk specimen (as the Cu case considered here), its size must be chosen large enough. To properly scale this problem, photoelectron waves leaving an emitter in free space decay in intensity with the inverse square of the distance from the emitter, i.e., as $1/r^2$: if there were no other damping effects, this would require an infinitely large cluster, since the number of scatterers on a shell at a given distance increases with the square of that distance, compensating the $1/r^2$ decay. Inelastic scattering adds an exponential decay factor, described theoretically by the inelastic attenuation length, which ensures that a finite

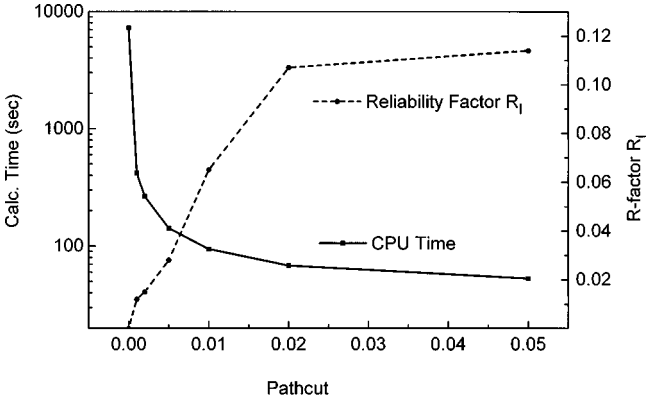

FIG. 8. Intensity reliability factor R_I [Eq. (14)] and calculation time on a 200 MHz Sun Sparc Ultra-2 workstation as a function of *pathcut*, for various choices of this parameter in second-order RA scanned-energy calculations for the 86-atom Cu(111) cluster. A value of 0 for *pathcut* corresponds to inclusion of all scattering events.

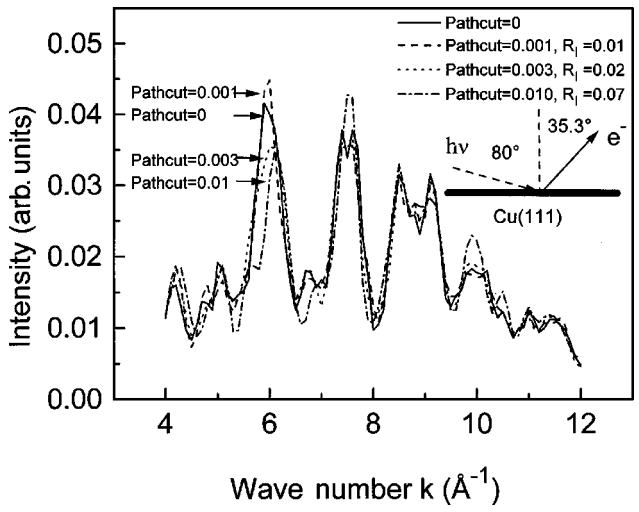

FIG. 9. Curve-to-curve comparisons of scanned-energy calculations for the 86-atom cluster and for different values of *pathcut*. Default values are used for other parameters.

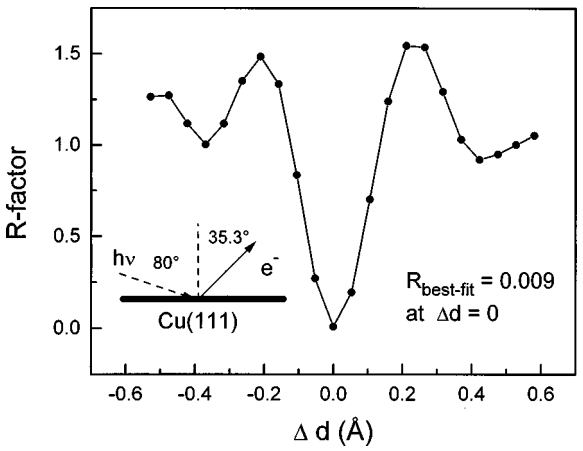

FIG. 11. Assessment of atomic position reliability of photoelectron diffraction calculations using the second-order RA approximation, shown by varying the first interlayer spacing and comparing to intensities calculated by using the exact formalism with zero interlayer relaxation. A cluster of 35 atoms was used.

cluster suffices. Vibrational effects and angular broadening act to further shrink the volume that is effective in producing diffraction modulations.

Figure 10 again shows scanned-energy results for the ideal clean Cu(111), but this time calculated for clusters of different sizes. The photon polarization angle is again 10° off-normal and the intensities are taken from the Cu 3p core level in the direction of normal emission, allowing emission

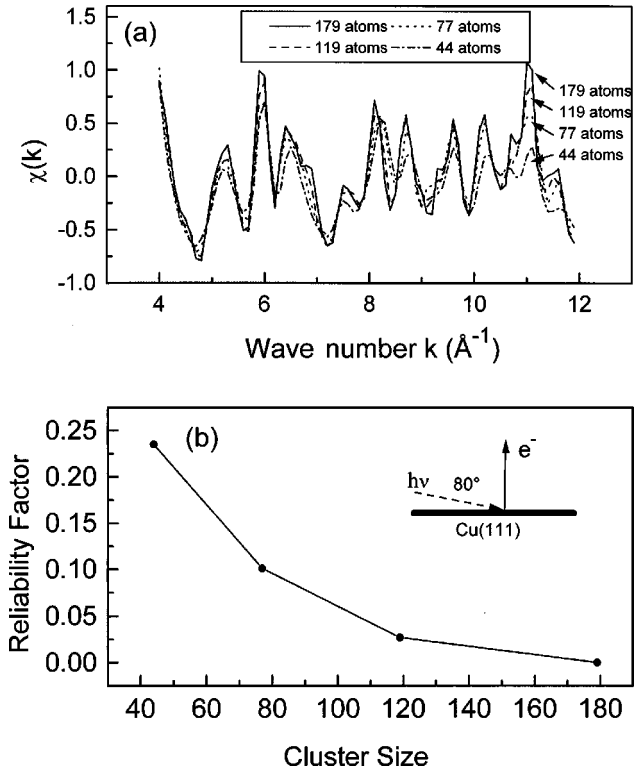

FIG. 10. (a) Effect of cluster size on scanned-energy calculated photoelectron diffraction χ (k)'s for Cu(111), with cluster sizes of 44, 77, 119, and 179 atoms. Default values are used for other parameters. (b) Reliability factor as a function of cluster size, with the 179-atom result used as the reference. See text for further details.

from all layers in the cluster. No *pathcut* is considered. To better compare these scanned-energy curves, we plot the usual $\chi(k)$ curves defined as

$$\chi(k)=[I(k)-I_0(k)]/I_0(k), \tag{15}$$

where $I(k)$ is the photoemission intensity at wave number k, and $I_0(k)$ is the background subtracted from the intensity versus wave number curve by using a spline fitting method. From Fig. 10 we can see that a 119-atom cluster yields most peaks and valleys at proper locations. Larger clusters become necessary for finer details. However, in practice, other effects not included here favor the sufficiency of smaller clusters: namely, vibrational damping of diffraction, and the experimental angular aperture (typically $\pm 3°$ to $\pm 5°$), both of which will tend to smooth out fine structure.

Thus, we conclude that clusters of about 100 atoms in size should be sufficient for most problems, in agreement with prior studies.[55–58]

V. RELIABILITY IN STRUCTRURE DETERMINATIONS

Finally, we consider the reliability with which such RA calculations can be used to determine atomic structures, using the classic approach of theory-experiment comparison via reliability factors or R factors. Although various definitions of R factors exist,[59,60] we will here use a rather straightforward definition of the goodness of fit between theory and experiment for photoelectron diffraction data:

$$R=\sum_i \frac{(\chi_{ci}-\chi_{ei})^2}{\chi_{ci}^2+\chi_{ei}^2}, \tag{16}$$

where χ_{ci} and χ_{ei} are calculated and experimental χ curves, respectively [cf. Eq. (14)]. As one way of estimating the reliability of the Rehr-Albers approximation for structure determinations, we have replaced the experimental data with the calculated scanned-energy (60–550 eV) results from the exact formalism, and based on a smaller 35-atom cluster representing Cu $3p$ emission from ideal clean Cu(111). We have used our RA method with RA order only up to 2 (6

$\times 6$ matrices) to explore sensitivity to possible variations in the outermost interlayer spacing by calculating the same scanned-energy curve and quantifying the fit to the exact result. The variation of R with interlayer spacing is shown in Fig. 11. It indicates a best fit R value of 0.009 at precisely the interlayer spacing that was used in the exact calculation, thus giving confidence in the ability of this method, even at second RA order, to accurately determine structure, while saving computer time. Our current implementation of the RA method with *pathcut* and adjustable orders should do even better than this.

VI. CONCLUSIONS

The Rehr-Albers (RA) separable propagator approximation up to fourth order [and using up to (15×15) matrices] has been applied to the calculation of photoelectron diffraction curves. By replacing the propagator matrices in the exact Green's-function formalism by the much smaller scattering-amplitude matrices of RA, this approximation saves much computation time. Our convergence tests for typical conditions in photoelectron diffraction indicate that fourth-order RA is highly accurate for all cases likely to be encountered. Furthermore, second-order RA [with (6×6) matrices] applied with clusters of 100 or more atoms and at least seventh-order multiple scattering, and using a *pathcut* of about 0.001, provides excellent results within 5% of ''exact'' results for most cases, particularly if the initial state is of s or p type. Higher Rehr-Albers orders are necessary for the first scattering events involved with initial states of d type (third order) and f type (fourth order), but can be neglected in later events. We have also implemented RA in a program that automatically adjusts the RA order from fourth downward according to the *pathcut* criterion, and this should permit fully quantitative and maximally efficient calculations for any situation. At least an order of magnitude in computation time is saved by recognizing that lower orders of Rehr-Albers suffice for most higher-order multiple scattering events. Larger clusters may be necessary for describing all fine structure in diffraction curves, but approximately 100 atoms should be the maximum needed for most cases. Looking ahead to future applications of the Rehr-Albers method, we note that several simulations of actual experimental data, e.g., on surfaces of W(110),[61] O/W(110),[62] Li/A(111),[63] and MnO(100),[64] etc., have also been performed using our program; these results will be published separately.

ACKNOWLEDGMENTS

This work was supported in part by the Director, Office of Energy Research, Basic Energy Sciences, Materials Sciences Division, of the U.S. Department of Energy under Contract No. DE-AC03-76SF00098, by LBNL Laboratory Directed Research and Development funds, by the National Energy Research Scientific Computing Center (NERSC), and by the Deutsche Forschungsgemeinschaft. We particularly thank Professor J. J. Rehr for insightful suggestions, comments, and discussions.

*Present address: California Air Resources Board, Sacramento, CA 95814.

[1] C. S. Fadley, M. A. Van Hove, Z. Hussain, and A. P. Kaduwela, J. Electron Spectrosc. Relat. Phenom. **75**, 273 (1995).
[2] C. S. Fadley, in *Synchrotron Radiation Research: Advances in Surface Science*, edited by R. Z. Bachrach (Plenum Press, New York, 1993).
[3] C. S. Fadley, Surf. Sci. Rep. **19**, 231 (1993).
[4] C. S. Fadley, S. Thevuthasan, A. P. Kaduwela, C. Westphal, Y. J. Kim, R. Ynzunza, P. Len, E. Tober, F. Zhang, Z. Wang, S. Ruebush, A. Budge, and M. A. Van Hove, J. Electron Spectrosc. Relat. Phenom. **68**, 19 (1994).
[5] S. A. Chambers, Adv. Phys. **40**, 357 (1990).
[6] D. A. Shirley, Y. Zhang, B. L. Petersen, Z. Hussain, W. A. Huff, J. J. Barton, and L. J. Terminello, J. Electron Spectrosc. Relat. Phenom. **68**, 49 (1994).
[7] H. P. Bonzel, Prog. Surf. Sci. **42**, 219 (1993).
[8] J. Osterwalder, P. Aebi, R. Fasel, D. Naumovic, P. Schwaller, T. Treutz, L. Schlapbach, T. Abukawa, and S. Kono, Surf. Sci. **331**, 1002 (1995).
[9] A. Szöke, in *Short Wavelength Coherent Radiation: Generation and Applications*, edited by D. T. Attwood and J. Bokor, AIP Conf. Proc. No. 147 (AIP, New York, 1986).
[10] J. J. Barton, Phys. Rev. Lett. **61**, 1356 (1988).
[11] G. R. Harp, D. K. Saldin, and B. P. Tonner, Phys. Rev. Lett. **65**, 1012 (1990).
[12] J. J. Barton, Phys. Rev. Lett. **67**, 3106 (1991).
[13] B. P. Tonner, Z.-L. Han, G. R. Harp, and D. K. Saldin, Phys. Rev. B **43**, 14 423 (1991).
[14] S. Y. Tong, C. M. Wei, T. C. Zhao, H. Huang, and H. Li, Phys. Rev. Lett. **66**, 60 (1991).
[15] S. Y. Tong and H. Huang, Phys. Rev. B **46**, 2452 (1992).
[16] H. Wu, G. J. Lapeyre, H. Huang, and S. Y. Tong, Phys. Rev. Lett. **71**, 251 (1993).
[17] H. Wu and G. J. Lapeyre, Phys. Rev. B **51**, 14 549 (1995).
[18] P. M. Len, F. Zhang, S. Thevuthasan, A. P. Kaduwela, C. S. Fadley, and M. A. Van Hove, J. Electron Spectrosc. Relat. Phenom. **85**, 145 (1997).
[19] K. Siegbahn, U. Gelius, H. Siegbahn, and E. Olsen, Phys. Lett. **32A**, 221 (1970).
[20] K. Siegbahn, U. Gelius, H. Siegbahn, and E. Olsen, Phys. Scr. **1**, 272 (1970).
[21] C. S. Fadley and S. Å. L. Bergström, Phys. Lett. **35A**, 375 (1971).
[22] C. S. Fadley, in *Progress in Solid State Chemistry*, Vol. 11, edited by G. A. Somorjai and J. O. McCaldin (Pergamon, New York, 1976) p. 265.
[23] R. J. Baird, C. S. Fadley, and L. F. Wagner, Phys. Rev. B **15**, 666 (1977).
[24] A. Liebsch, Phys. Rev. Lett. **32**, 1203 (1974).
[25] A. Liebsch, Phys. Rev. B **13**, 544 (1976).
[26] C. H. Li and S. Y. Tong, Phys. Rev. Lett. **42**, 901 (1979).
[27] J. B. Pendry, Surf. Sci. **57**, 697 (1976).
[28] C. H. Li, A. R. Lubinsky, and S. Y. Tong, Phys. Rev. B **17**, 3128 (1978).
[29] S. Kono, S. M. Goldberg, N. F. T. Hall, and C. S. Fadley, Phys. Rev. Lett. **41**, 1831 (1978).
[30] S. Kono, S. M. Goldberg, N. F. T. Hall, and C. S. Fadley, Phys. Rev. B **22**, 6085 (1980).
[31] L.-G. Peterson, S. Kono, N. F. T. Hall, C. S. Fadley, and J. B. Pendry, Phys. Rev. Lett. **42**, 1545 (1979).
[32] J. J. Barton and D. A. Shirley, Phys. Rev. B **32**, 1892 (1985).

[33] J. J. Barton and D. A. Shirley, Phys. Rev. B **32**, 1906 (1985).
[34] P. Lloyd and P. V. Smith, Adv. Phys. **21**, 69 (1972).
[35] A. Chassé, Ph.D. thesis, University of Halle, 1984.
[36] P. Rennert and A. Chassé, Exp. Tech. Phys. (Berlin) **35**, 27 (1987).
[37] F. J. García de Abajo, A. Chassé, Y. Chen, M. A. Van Hove, and C. S. Fadley (unpublished).
[38] J. J. Barton, Ph.D. thesis, University of California, Berkeley.
[39] V. Fritzsche and P. Rennert, Phys. Status Solidi B **135**, 49 (1986).
[40] A. Chassé, Surf. Sci. **213**, 648 (1988).
[41] P. Rennert and N. Van Huang, Phys. Status Solidi B **148**, 49 (1988).
[42] J. J. Rehr and R. C. Albers, Phys. Rev. B **41**, 8139 (1990).
[43] A. P. Kaduwela, D. J. Friedman, and C. S. Fadley, J. Electron Spectrosc. Relat. Phenom. **57**, 223 (1991).
[44] Y. Chen, H. Wu, and D. A. Shirley (unpublished).
[45] Y. Chen and M. A. Van Hove (unpublished); The MSCD program package is available at http://electron.LBL.gov/mscdpack/.
[46] F. Manar and C. Brouder, Physica B **208/209**, 79 (1995).
[47] D. Sébilleau, J. Phys.: Condens. Matter **7**, 6211 (1995).
[48] M. A. Van Hove, A. P. Kaduwela, H. Xiao, W. Schattke, and C. S. Fadley, in *Proceedings of the 11th International Conference on Vacuum Ultraviolet Radiation Physics* [J. Electron Spectrosc. **80**, 137 (1996)].
[49] M. Biagini, Phys. Rev. B **46**, 10 588 (1992).
[50] P. A. Lee and J. B. Pendry, Phys. Rev. B **11**, 2795 (1975).
[51] M. Biagini, Phys. Rev. B **48**, 2974 (1993).
[52] V. L. Moruzzi, J. F. Janak, and A. R. Williams, *Calculated Electronic Properties of Metals* (Pergamon Press, New York, 1978).
[53] S. Tanuma, C. J. Powell, and D. R. Penn, Surf. Interface Anal. **20**, 77 (1993).
[54] C. J. Powell, A. Jablonski, S. Tanuma, and D. R. Penn, J. Electron Spectrosc. Relat. Phenom. **63**, 605 (1994).
[55] C. S. Fadley, in *Synchrotron Radiation Research: Advances in Surface and Interface Science, Volume 1: Techniques*, edited by R. Z. Bachrach (Plenum Press, New York, 1992), p. 421.
[56] M. Sagurton, E. L. Bullock, and C. S. Fadley, Phys. Rev. B **30**, 7332 (1984).
[57] M. Sagurton, E. L. Bullock, and C. S. Fadley, Surf. Sci. **182**, 287 (1987).
[58] L. J. Terminello, X. S. Zhang, Z. Q. Huang, S. Kim, A. E. Schach von Wittenau, K. T. Leung, and D. A. Shirley, Phys. Rev. B **38**, 3879 (1988).
[59] M. A. Van Hove, S. Y. Tong, and M. H. Elconin, Surf. Sci. **64**, 85 (1977).
[60] M. A. Van Hove, W. H. Weinberg, and C.-M. Chan, *Low Energy Electron Diffraction: Experiment, Theory and Surface Structure Determination* (Springer-Verlag, Berlin, 1986).
[61] R. Ynzunza, Y. Chen, F. J. Palomares, E. D. Tober, H. Daimon, Z. Wang, J. Liesegang, Z. Hussain, M. A. Van Hove, and C. S. Fadley (unpublished).
[62] R. Ynzunza, Y. Chen, F. J. Palomares, E. D. Tober, H. Daimon, Z. Wang, J. Liesegang, Z. Hussain, M. A. Van Hove, and C. S. Fadley (unpublished).
[63] G. Zhuang, Y. Chen, X. Zhou, M. A. Van Hove, and P. N. Ross (unpublished).
[64] J. Rigolini, G. Biino, A. Kay, S. Mun, C. Westphal, Y. Chen, H.-C. Siegmann, M. A. Van Hove, and C. S. Fadley (unpublished).